Doppler Lidar observations over a high altitude mountainous site Manora Peak in the central Himalayan region

D. V. Phanikumar[1], K. K. Shukla[1,2], M. Naja[1], N. Singh[1], S. Sahai[3], R. Sagar[1], S. K. Satheesh[4,5], K. K. Moorthy[4], V. R. Kotamarthi[6] and Rob K. Newsom[7]

[1]Aryabhatta Research Institute of Observational Sciences, Nainital 263 002, India
[2]Pt. Ravishankar Shukla University, Raipur 492 010, India
[3]Amity University, Noida 201 303, India
[4]Centre for Atmospheric and Oceanic Sciences, Indian Institute of Science, Bengaluru 560 012, India
[5]Divecha Centre for Climate Change, Indian Institute of Science, Bengaluru 560 012, India
[6]Argonne National Laboratory, Argonne, IL, USA
[7]Pacific Northwest National Laboratory, Richland, Washington, USA

The RAWEX–GVAX field campaign has been carried out from June 2011 to March 2012 over a high altitude site Manora Peak, Nainital (29.4°N; 79.2°E; 1958 m amsl) in the central Himalayas to assess the impacts of absorbing aerosols on atmospheric thermodynamics and clouds. This paper presents the preliminary results of the observations and data analysis of the Doppler Lidar, installed at Nainital. Strong updrafts with vertical winds in the range of ~2–4 ms^{-1} occurred during the daytime and throughout the season indicating thermally driven convection. On the other hand during nighttime, weak downdrafts persisted during stable conditions. Plan Position Indicator scan of Doppler Lidar showed north-northwesterly winds in the boundary layer. The mixing layer height, derived from the vertical velocity variance, showed diurnal variations, in the range ~0.7–1 km above ground level during daytime and very shallow during nighttime.

Keywords: Boundary layer, Doppler Lidar, GVAX.

Introduction

THE atmospheric boundary layer (ABL) is an important part of the atmosphere which acts like as a conduit between the Earth's surface and free atmosphere[1]. Pollutants, natural and man-made, are spatially re-distributed by the ABL dynamics[2], while their radiative interactions would affect the ABL also[3,4]. The pollutants in the nearby valley region are transported from the surface to higher altitudes through convective mixing and terrain forcing. These forces vary geographically (low-latitude, mid-latitude and poles), topographically (terrain, continental, marine and soil), dynamically (large scale vertical motion and advection) and biologically (forest, agricultural, desert)[1,5]. Manora Peak (29.4°N; 79.2°E; 1958 m above mean sea level (amsl)), in Nainital is a high altitude site in the central Himalayas, is located above the ABL of the valley and plains, and thus could be considered as a free-tropospheric site and regional representative for the northern India[5–8] at least during some part of the year. Because of its unique topography and the strong diurnal variations in aerosols observed at the site[6] caused by the ABL evolution, and terrain-induced cloud formation in addition to synoptic scale monsoon cloud systems, this site provides an interesting opportunity to measure and evaluate cloud–aerosol interactions in the Ganges valley region of Indian-subcontinent. In order to study the ABL processes and cloud, we need very precise measurements of winds and turbulence, which is made possible by Doppler Lidar (DL)[9] and supporting measurements. In order to validate the wind speed and direction derived from the DL data, we have launched the radiosonde (RS) at synoptic hours (00, 06, 12 and 18 UT) during the campaign period from the site.

The field campaign Regional Aerosols Warming Experiment–Ganges Valley Aerosol Experiment (RAWEX–GVAX) has been conducted at Manora Peak, Nainital, during June 2011–March 2012 to study the impact of aerosols and clouds in the Earth's radiation budget. It has been an Indo-US collaborative effort, during which Atmospheric Radiation Measurement (ARM) Climate Research Facility (US), mobile Facility (AMF) was installed at the Manora Peak. The DL formed part of this campaign and has been operated continuously during the observational period aiming at characterizing the ABL evolution, aerosols and clouds. Such a facility has been operated for the first time at a high altitude site in India, and this paper presents the details of the analysis of the DL data and the preliminary findings on the ABL over the observational site.

*For correspondence. (e-mail: phani@aries.res.in)

Topography and general meteorology around the site

The latitude–longitude topography of the Indian subcontinent with the observational site (represented by the black open star) is shown in Figure 1. This site is considered as the regional representative of aerosol concentration and trace gases in the Indo-Gangetic Plain (IGP) region. During the GVAX period, the highest temperature is observed during monsoon and pre-monsoon seasons 20°C and the lowest temperature is observed in winter season (12°C). The maximum humidity is observed in monsoon and minimum in pre-monsoon. Westerly (easterly) winds are dominant during winter (monsoon) seasons over the site. The general meteorology around the site is discussed elsewhere[8,10].

Instrumentation

Doppler Lidar

The Doppler Lidar (DL) is an optical analog of the Doppler radar[11] and has been fabricated by the Halo-Photonics[12]. It has a monostatic configuration, with an eye-safe, solid state laser of wavelength 1.5 μm having a pulse energy (~100 μJ) and high pulse repetition rate (~15 kHz) as transmitter. The DL receiver provides the vertical profile of the atmosphere up to ~9.6 km (320 range bins) with the range resolution of 30 m. The signal detection employs a heterodyne technique[13,14] and the resulting Doppler frequency spectra can be used to derive the winds (m s^{-1}) as well as to estimate the attenuated backscatter (m^{-1} sr^{-1}). The detailed description of the system is given elsewhere[12,15] and the essential technical specifications are summarized in Table 1.

The horizontal as well as vertical and 3-D scan of winds in the atmosphere can be done by DL. It can scan the atmosphere in three different scanning modes, i.e. fixed beam stare (FPT), range-height indicator (RHI) and plan position indicator (PPI); respectively indicating the atmosphere vertically, elevationally (once every 2 h) and azimuthally (once every 1 h)[15]. For the rest of the time, DL operated vertically in fixed beam stare mode when the other two (PPI & RHI) scans are not performed. FPT scan mode provides the signal-to-noise ratio (SNR), vertical velocity and attenuated backscatter (β) of the atmosphere. In RHI scan mode, the DL sampled the atmosphere using a step-stare scanning method at a constant azimuth angle of 201.5° and an elevation increment of 2°. RHI scan provides a better understanding of the aerosol transport from nearby valley regions over the site. For a 3-D map of atmospheric wind, PPI scan mode of the DL sampled the atmosphere using a step-stare scanning method at a constant elevation angle of 24° and an azimuth increment of 5°.

The line of sight (LOS) or radial wind velocity is estimated using the Doppler shift observed using aerosols as a tracer. Under the clear-sky condition, DL gives accurate measurements of radial velocity with a precision of ~10 cm s^{-1}. The Lidar is housed in a temperature and humidity controlled enclosure. The transceiver optics and the onboard computer are housed in the main enclosure. A sample photograph of DL is shown in Figure 2. The operation of DL depends on the atmospheric conditions and Lidar parameters[16,17]. The 3-D scan of the atmosphere provides the zonal (u) and meridional (v) mean wind components of the atmosphere by using velocity–azimuth display (VAD) technique[18]. By using zonal and meridional wind component, wind speed and wind direction can be estimated.

In the present study, we have used the level b1 (the quality control (min/max/delta) checks applied to measurements) data. The description of the data quality can be found at http://www.archive.arm.gov/docs/BrowserDoc/Glossary/index.htm#datalevel. Vertical profile of

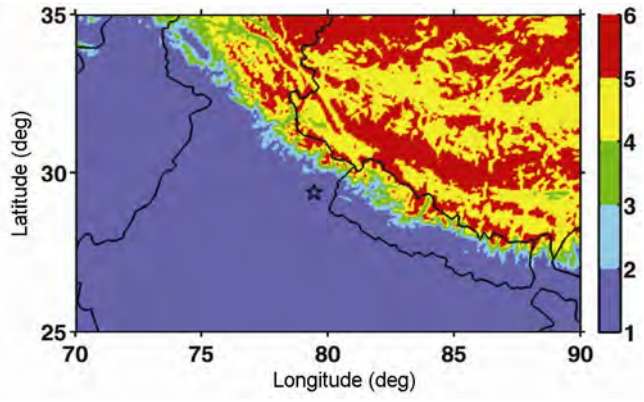

Figure 1. Topography of the Indian subcontinent over which the GVAX is conducted. The black open star represents the observational site Manora Peak, Nainital.

Table 1. Parameters of the Doppler Lidar

Manufacturer	Halo photonics
Eye safety	Class 1M
Wavelength	1.5 μm
Laser pulse energy	~100 μJ
Laser pulse width	150 ns (22.5 m)
Pulse rate	15 kHz
Nyquist velocity	19.4 m/s
Unambiguous range	10 km
Aperture	75 mm
Volume approximately	0.5 m^3
Power consumption	<300 W
Mass approximately	85 kg
Temporal resolution (selectable)	0.1 to 30 s
Range gate size	18 to 60 m
Velocity precision	<20 cm/s for SNR > –20 dB
Minimum range	<100 m, typically 75 m
Scanning	Step-stare, full upper hemisphere
Enclosure	Weatherproof, temperature stabilized

SNR is considered for estimating the appropriate threshold for SNR. The mean of SNR at range, r_j has been taken to measure the velocity precisely, i.e.

$$\mathrm{SNR}_j = \frac{1}{N}\sum_{i=0}^{N-1}\mathrm{SNR}_{ij}, \quad (1)$$

where j represents the height range bin and i represents the time bin (1 to N sec) and summation is over (i) that implies it is temporally averaged over the selected duration, for each of the range bins[19].

Retrieval method of the wind speed and direction

To estimate the wind component, we have used the data from 3-D PPI scans and also used VAD technique[18,19]. We have assumed velocity fields to be horizontally homogeneous within each height range bin[20]. By using u and v component, we can estimate the wind speed and direction by using the equations

$$\text{Wind speed} = \sqrt{u^2 + v^2}, \quad (2)$$

$$\text{Wind direction (deg)} = 180 \times \frac{(\arctan\frac{u}{v} + \mathrm{pi})}{\mathrm{pi}}. \quad (3)$$

Radiosonde

The radiosonde (RS92-SGPD RS) from Väisälä has been launched at regular intervals during the campaign at 00, 06, 12 and 18 UT for the vertical profiling of atmospheric thermodynamics (i.e. temperature, wind speed and relative humidity) parameters. The normal ascent rate of the balloon is 5 ms^{-1}, transmitter time resolution is 2 sec and the vertical resolution of the RS data is 10 m. To compare the wind speed estimated by DL with RS, we have interpolated the RS data with 30 m resolution.

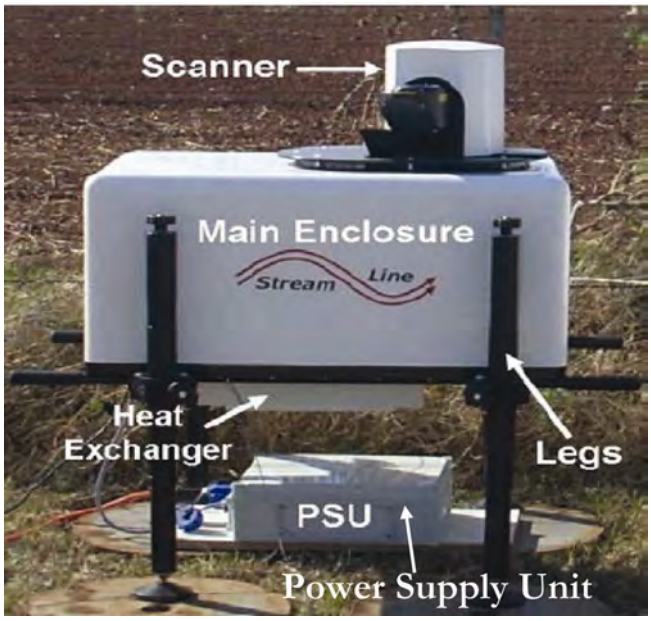

Figure 2. Mechanical appearance of Doppler Lidar.

Results and discussion

The first step towards analysis of the data noise is to remove the outliers. A typical case is shown in Figure 3, where the vertical profiles of SNR for 02 December 2011 at 06 UT (11 : 30 IST) and for 23 September 2011 at 19 UT (00 : 30 IST) are shown. While the former is representative of fully developed daytime convective conditions, the latter represents typical stable nocturnal conditions. The raw data in Figure 3 shows significant noise content. In order to remove the noise from the data, initial data quality check is done by fixing a threshold for the SNR. We varied the SNR from –15 dB to –25 dB and found the –20 dB to be an appropriate threshold for all scans. Therefore, we applied a threshold of –20 dB for all types of scans (FTP, RHI and PPI) of the DL which can considerably reduce the noise level[12,21,22]. To have a better understanding on the relationship between SNR and vertical velocity during convective and stable conditions, we have selected two times; one during local noon, 07:00 UT (12 : 30 IST) and the other around midnight 19 : 00 UT (00 : 30 IST). Figure 4 *a* shows the daily variation of the SNR and vertical velocity at different altitudes on 12 : 30 IST. We have taken three different heights in the ABL 0.5 km (represented by green open circle), 1 km (represented by black open triangle) and 1.5 km (represented by red down open triangle) above ground level (AGL) to assess the basic characteristics of the signal in daytime convective conditions. Positive Doppler velocity implies that the targets moving away from the DL (updraft) and negative Doppler velocity implies that the targets approaching the DL (downdraft). It is clearly evident from the figure that SNR decreases with increasing height due to the high aerosol concentration at lower altitudes and less concentration in higher altitudes in the atmosphere. Our observations show the presence of strong updrafts at lower altitudes, decreasing at higher levels. During nocturnal stable conditions of the atmosphere for the same observational period, Figure 4 *b* shows the daily variation of the SNR and vertical velocity at altitudes 0.5, 1 and 1.5 km, AGL at 00 : 30 IST. It is noticed from the figure that the SNR is stronger in lower altitudes than higher altitudes and the dominance of downdrafts is clearly observed during stable conditions. The Figure clearly shows stronger updrafts with vertical motions in the 1–3 m s^{-1} range during the daytime, prevailing even at altitudes as high as 1000 m, during clear sunny periods of December–March. On the other hand, during nighttime, the ABL is benign, and calm, with vertical motions

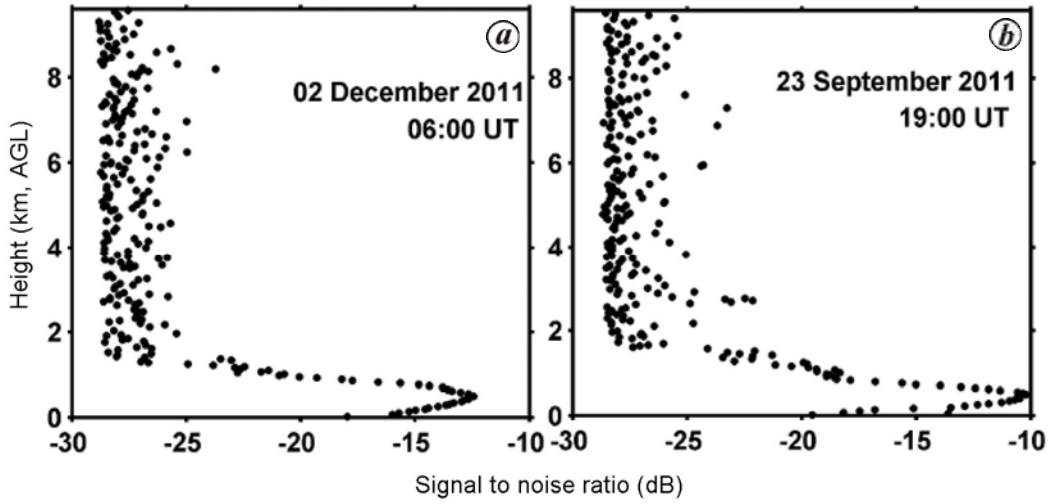

Figure 3. Vertical profiles of DL signal-to-noise ratio (SNR). ***a***, For a typical convective condition on 2 December 2011 at 06 : 00 UT (11 : 30 IST); ***b***, For the nocturnal stable condition on 23 September 2011 at 19 : 00 UT (00 : 30 IST). We have observed the less noisy data up to 2 km, AGL over the site in both convective and stable atmosphere.

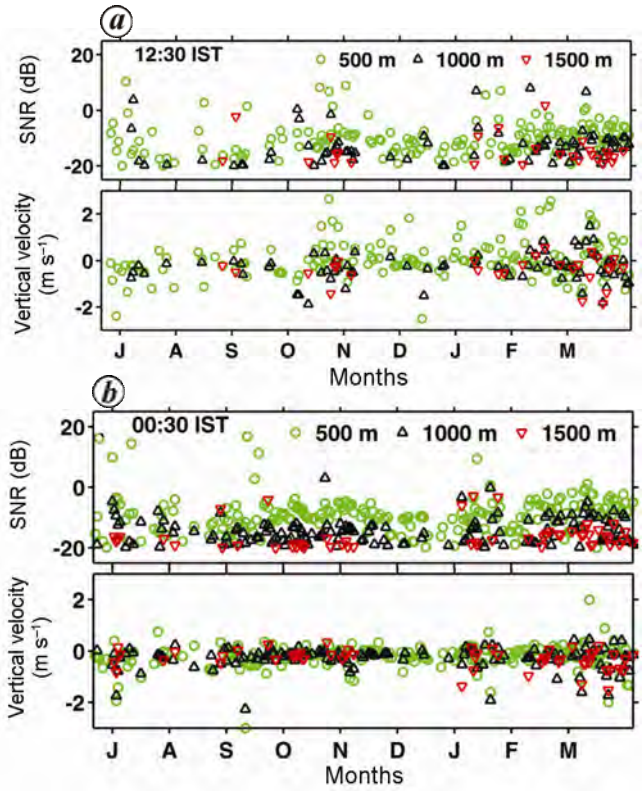

Figure 4. Time series of daily mean SNR and vertical velocity (m s^{-1}) (***a***) during strong convective period during daytime 07 : 00 UT (12 : 30 IST) and (***b***) for the stable conditions around midnight 19 : 00 UT (00 : 30 IST). The convective updrafts are stronger during daytime and at lower altitudes. The magnitudes of updrafts are the least during the rainy monsoon months and start increasing from November reaching their peak values by March.

$< \pm 1$ ms^{-1} and confined only to the lower altitude (500 m) during any month of the observational period. The observed short-period modulations are attributed to the orography effects. This aspect will be studied in detail and left for future work.

Diurnal variation of SNR, vertical velocity and attenuated backscatter (β)

The lower most part of the atmosphere (100–3000 m, amsl) represents the ABL, where turbulent motions would modify the mean flow[1]. To perceive the diurnal variation of the SNR, vertical velocity and attenuated backscatter (β) in the ABL, we have taken as an example 2 December 2011. Figure 5 *a–c* shows the diurnal variation of 10-min averaged SNR, vertical velocity and attenuated backscatter. The figure reveals the diurnal evolution of well-defined structure of the ABL over the land. The ABL is subdivided into three different sublayers such as mixed layer (ML), residual layer (RL) and stable boundary layer (SBL). The ML is also known as a convective boundary layer (CBL)[1]. The development of ML can be observed in Figure 5 *a–c* in which the DL signal enhances during the 04 : 00 UT–08 : 00 UT (09 : 30 to 13 : 30 IST). The main source behind the development of ML is convection, which is driven by the diurnal solar heating (06 : 49 IST). The transport of the aerosols and thermals associates with the upslope wind motion during daytime over the site[8]. From Figure 5 *b*, it is observed that the thermal plumes (containing aerosols and other atmospheric pollutants) start rising from early morning to the afternoon up to a maximum mixing height of ~700 m attained at 07 : 00 UT (12 : 30 IST), due to diurnal solar heating and starts collapsing from evening 10 : 00 UT (15 : 30 IST), becoming stable during nighttime 21 UT (02 : 30 IST). The maximum rise during daytime ABL on sunny days exceeded ~700 m, even though Figure 5 *b* has shown the active convection during 4.5–7.5 UT (10.2–13.2 IST). The RL is the second important layer of the ABL, which is formed due to lower surface heating after sunset. The RL appears as time progresses and descend down to 0.3 km at about 13 : 00 UT (18 : 30 IST). Moreover, eddies move

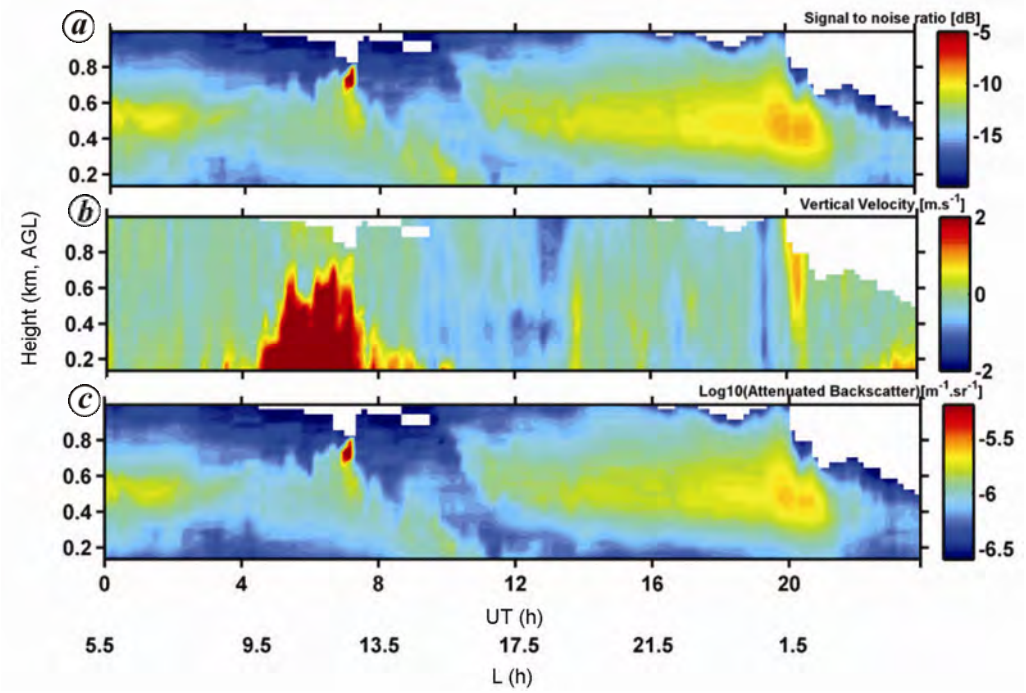

Figure 5. Diurnal variation of 10-min averaged (***a***) SNR, (***b***) vertical velocity and (***c***) attenuated backscatter data on 2 December 2011 over Manora Peak.

downward as the night progresses and turbulence weakens considerably due to negative buoyancy leading to the formation of a stable stratified region near the ground. However, we see SBL which is at a height of ~0.3–0.5 km usually in the nighttime 13–24 UT (18 : 30–05 : 30 IST)[23]. While the daytime convection is signified by persistent updraft, the stable conditions represent alternating up and down drafts, which are very weak. It is clear from Figure 5 *c* that we have observed strong aerosol backscatter during 11–21 UT (16 : 30–02 : 30 IST). To know the cause in the increase of aerosol backscatter during evening hours, we have plotted the vertical profile of the potential temperature (PT) (solid black line) and relative humidity (RH) (solid green line) at synoptic hours 00, 06, 12 and 18 UT in Figure 6 *a–d* on 2 December 2011 respectively. The vertical profile of RH indicates the conditions conducive for activating the aerosols to cloud condensation nuclei (CCN) and PT indicates the unstable/stable condition in the atmosphere. The increase of RH at 12 UT could give us a hint about the nature of aerosols over the central Himalayan region. The increase in aerosol backscatter cross section during evening hours may be associated to the hygroscopic nature of aerosols over the site. However, this aspect needs to be studied further with suitable datasets and will be dealt as a separate study. Similarly, we have observed the stable condition up to 0.6 km in nighttime with high RH (Figure 6 *d*) and observed the strong backscatter by DL in Figure 5 *c* and after 22 UT, we have observed the stable layer which suspected that the cooling is a combination of the downdraft, subsidence and cool advection of the moist air over the site.

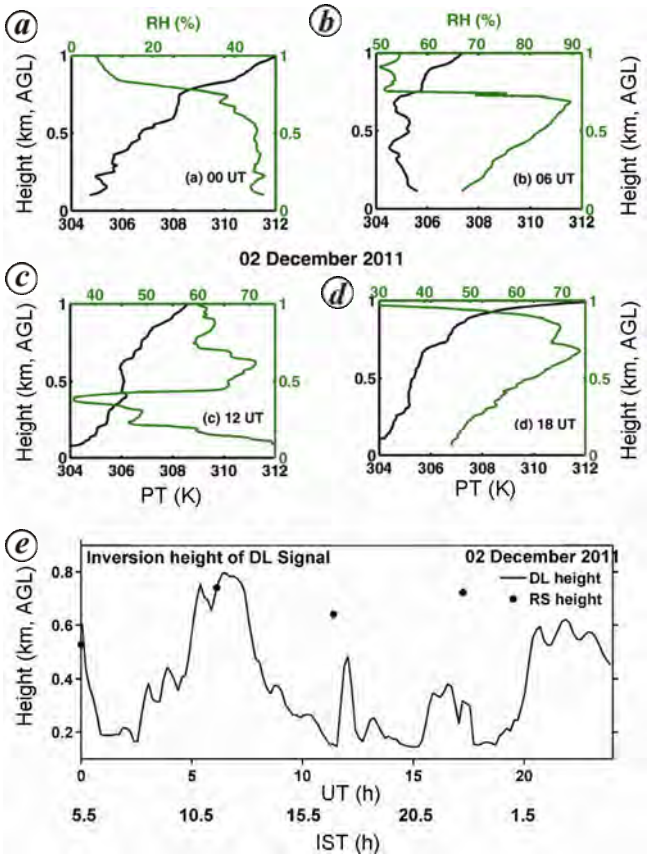

Figure 6. ***a–d***, Vertical profiles of the potential temperature and relative humidity (RH) on 2 December 2011, derived from the radiosonde ascents at 00, 06, 12 and 18 UT show the convection dominated feature; (***e***), Diurnal variation of inversion or mixing layer height of DL on 2 December 2011.

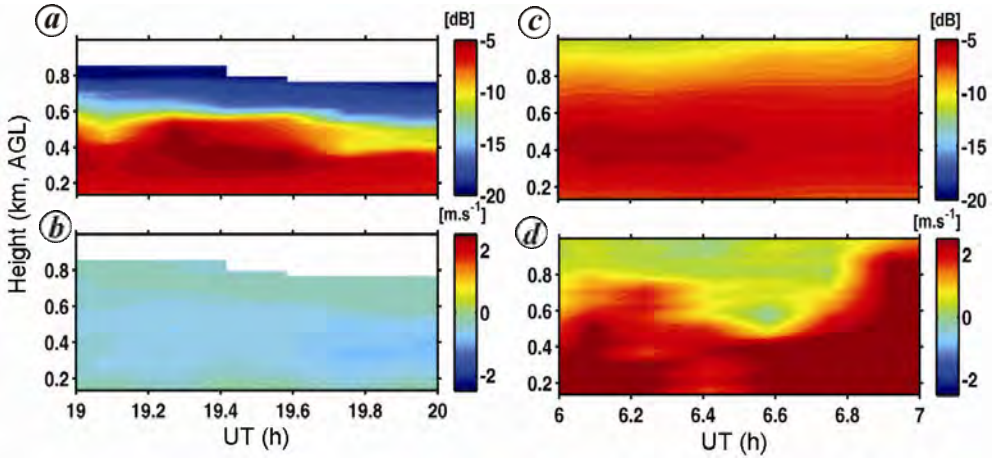

Figure 7. ***a***, ***b***, Height–time variation of SNR (dB) and vertical velocity (m s^{-1}) in (***a***, ***b***) stable condition on 10 March 2012 from 19 : 00 to 20 : 00 UT (00 : 30–01 : 30 IST). ***c***, ***d***, Height–time variation of SNR (dB) and vertical velocity (m s^{-1}) in convective condition 10 March 2012 from 06 : 00 to 07 : 00 UT (11 : 30–12 : 30 IST).

We have estimated the inversion or mixing layer height by using vertical velocity variance data of DL on 2 December 2011 (Figure 6 *e*). To estimate the inversion or mixing layer height from the DL signal, we have used the wavelet-covariance transform (WCT) method and detailed description about the WCT can be found elsewhere[22]. The dilation is used 150 m for the 2 December 2011 in WCT. The inversion or mixing layer height observed by DL shows the diurnal variation on 02 December 2011 throughout the day. We have also estimated the inversion or mixing layer height from the PT gradient of RS on 2 December 2011 at 00, 06, 12 and 18 UT. We have compared the inversion layer height estimated from DL (solid black line) and RS (filled circle) in Figure 6 *e*. The inversion layer height from DL and RS at 00 and 06 UT shows the same height, but some discrepancies are observed at 12 and 18 UT. RS shows higher inversion layer height in comparison to DL.

Variation in vertical velocity

The local weather is directly influenced by the growth and decay of the ABL and increasing the depth of ABL also shows the convective activity in the atmosphere[24]. ABL depth is also influenced by the wind dynamics around the site. In order to see the general characteristics of vertical velocity during stable and convective atmosphere, we have taken 10 March 2012 from 00 : 30 to 01 : 30 IST (19 : 00–20 : 00 UT) for stable condition and 10 March 2012 at 11 : 30–12 : 30 IST (06 : 00–07 : 00 UT) for convective condition (Figure 7 *a–d*). White pixel shows the removal of the noise from the SNR and vertical velocity by applying an appropriate threshold (–20 dB). Figure 7 *a–b* shows the height–time variation of SNR (dB) and vertical velocity (m s^{-1}) on 10 March 2012 from 00 : 30 to 01 : 30 IST (19 : 00–20 : 00 UT) plotted from FPT scan mode data to show the stable condition of the atmosphere which essentially represents the background signal and corresponding vertical velocities. Figure 7 *c–d* shows the height–time variation of SNR (dB) and vertical velocity (m s^{-1}) on 10 March 2012 from 11 : 30 to 12 : 30 IST (06 : 00–07 : 00 UT) plotted from FPT scan mode data to show the convective condition of the atmosphere. Figure 7 *d* shows the dominant upslope flow over the site during the noon hours and vertical velocity varies between 3 and 4 m s^{-1} in the mixing layer height. Figure 7 *b* shows that the vertical velocities are constant and close to zero, which is the case of stable atmosphere. During nighttime, downslope (negative velocity) winds are more dominant, which is evident from Figure 7 *b* (ref. 12). In order to see the mean picture of vertical velocity in convective (06–07 UT) and stable (19–20 UT) condition, we have taken the mean of 0.1–0.5 and 0.5–1 km for 1 h 10 min averaged data of 10 March 2012. Figure 8 shows that the vertical velocity is stronger in magnitude (upward velocity) in the ABL than the free atmosphere. In case of stable condition, it is downward and close to zero[20].

RHI and PPI scan of the atmosphere by DL

To study aerosol transport from the valley to the site at the Manora peak by wind and also wind dynamics, we have taken 23 September 2011 as an example for both the RHI and PPI mode scan. Figure 9 *a, b* shows the altitude, ground range variation of the SNR and radial velocity for RHI mode. Figure 9 *c, d* shows the variation of SNR and radial velocity. White pixels represent the removal of the bad data by using the threshold condition. RHI scan performed over the site could assist understanding how the pollutants from the nearby valley regions are transported over the elevated site. The ground range is the horizontal

distance from the Lidar to a given sample point. A strong signal is not observed in near vertical direction, but found at higher elevation angles and can be interpreted as the aerosol transport from nearby valley regions during daytime boundary layer evolution over the central Himalayan region. The time chosen in PPI scan is nighttime, which shows the different characteristics of the stable atmosphere[11]. Radial velocity near the surface shows the north-northwesterly wind. The thermal plumes in the ABL start developing in the morning, which can be clearly seen in the PPI scan (Figure 9 *b*).

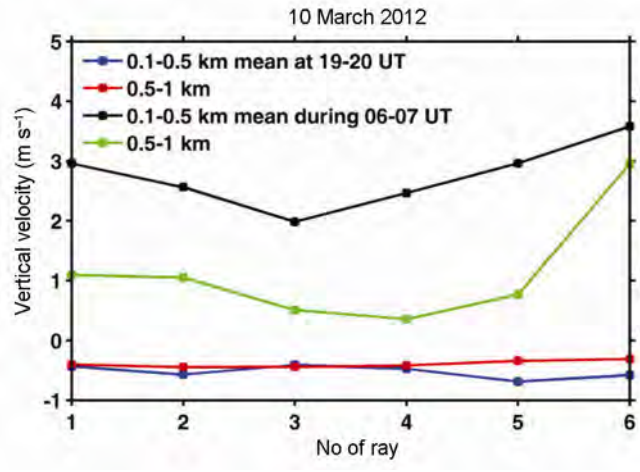

Figure 8. 10 min averaged vertical velocity during convective and stable condition on 10 March 2012 (06–07 UT; black and green lines) and (19–20 UT; blue and red lines). Note the higher updrafts under convective conditions.

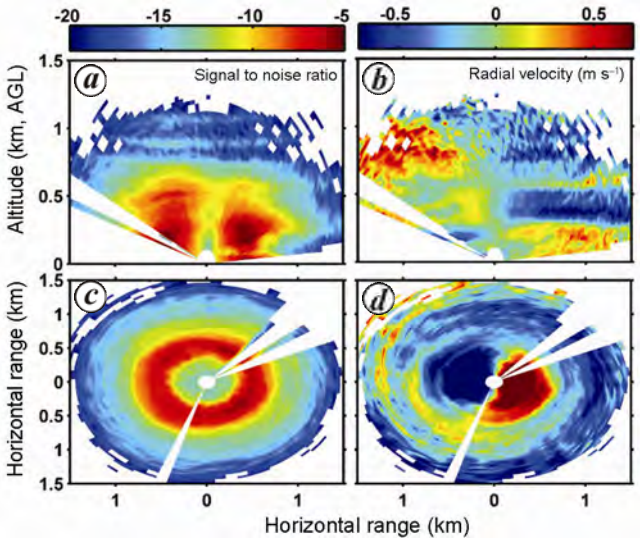

Figure 9. ***a***, ***b***, Altitude, ground range or horizontal range variation of the SNR and radial velocity for RHI scan mode of the DL at 19 UT. ***c***, ***d***, Variation of SNR and radial velocity with respect to the altitude in *x* (east) direction and *y* (north) direction of PPI scan mode at 19 UT.

Comparison of wind speed derived from the PPI scan

Figure 10 shows the comparison between the vertical profile of wind speed derived from DL (solid black line) and RS (dotted red line) at synoptic hours (00, 06, 12 and 18 UT) on 19 October 2011 respectively. The DL-estimated wind speed[25–27] at the synoptic hours has been compared with RS wind speed at the same time. As we have DL wind speed profile at a vertical resolution of 30 m and to compare it with RS, we have interpolated RS data at 30 m range resolution. Westerly winds are dominant over the site during winter and the balloon drifted into nearby country Nepal[10]. Balloons drift over the northern Indian region during the pre-monsoon and post-monsoon seasons[10]. The co-relation is reasonably good below ~1 km between DL and RS, however, large differences are observed above 1 km which could be the result of the drift of RS by higher wind speeds thereby increase in spatial separation between DL and RS. The atmospheric variations as well as the random error and bias of radial velocity measurements are used to measure accurately the horizontal velocity[9]. It can be clearly seen Figure 10 that the wind speed from two different instruments is well correlated and is within the expected error bounds at synoptic hours (00, 06, 12, 18 UT). It should also be noted that the inter-comparison between two instruments will be affected by different spatial and temporal resolution of the measurements which encounter with different atmospheric conditions and dynamics[12].

Summary and conclusions

The preliminary results from the DL experiment reveal some key facts about the transport of aerosols over the

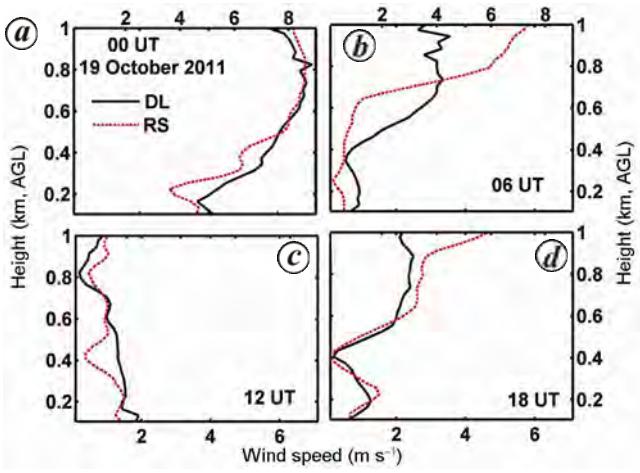

Figure 10. Comparison of wind speed derived from DL PPI scan and RS for 19 October 2011 at (***a***) 00 UT (05 : 30 IST), (***b***) 06 UT (11 : 30 IST), (***c***) 12 UT (17 : 30 IST) and (***d***) 18 UT (23 : 30 IST). The solid black line represents DL wind speed and dotted red line represents RS wind speed.

site and wind dynamics around the central Himalayan region that could be used as input parameters for constraining model simulations over the IGP region. An appropriate SNR threshold (–20 dB) is observed for the vertical velocity and attenuated backscatter of DL. Vertical velocities have greater amplitude (~2–4 ms^{-1}) during convective condition and have almost constant amplitudes during stable condition. Updrafts are observed during the convection period due to surface heating by the Sun and downdrafts are observed during a stable condition of the atmosphere due to surface cooling. The mixing layer height observed by the DL during daytime is ~0.7–1 km AGL and observed SBL during nighttime is usually ~0.3–0.4 km AGL over the central Himalayas.

RHI scan shows that the radial velocities became strong as we move towards the higher elevation angles and varies ~± 1 m s^{-1} which is because of the dynamics of the central Himalayan region. It also reveals the transport of aerosols from the nearby valley region over the site due to the upslope wind and mountain-valley breeze. PPI scan shows that the wind in the ABL near the surface is north-northwesterly. The data of the derived wind speed from DL and RS are well correlated with magnitude and time in the ABL. The detailed analysis of DL data is in progress.

1. Stull, R. B., *An Introduction to Boundary Layer Meteorology*, Springer Science, 1988.
2. Kaufman, Y. J., Passive remote sensing of tropospheric aerosol and atmospheric correction for the aerosol effect. *J. Geophys. Res.*, 1997, **102**(D14), 16815–16830.
3. Garratt, J. R., Sensitivity of climate simulations to land–surface and atmospheric boundary-layer treatments – a review. *J. Clim.*, 1993, **6**, 419–448.
4. Tegen, I., Lacis, A. A. and Fung, I., The influence on climate forcing of mineral aerosols from disturbed soils. *Nature*, 1996, **380**, 419–422.
5. Sagar, R., Kumar, B., Dumka, U. C., Moorthy, K. K. and Pant, P., Characteristics of aerosol spectral optical depths over Manora Peak: a high-altitude station in the central Himalayas. *J. Geophys. Res.*, 2004, **109**, D06207.
6. Dumka, U. C., Satheesh, S. K., Pant, Hegde, P and Krishna, M. K., Surface changes in solar irradiance due to aerosols over central Himalayas. *Geophys. Res. Lett.*, 2006, **33**, L20809.
7. Kumar, R., Naja, M., Venkataramani, S. and Wild, O., Variations in surface ozone at Nainital: a high altitude site in the central Himalayas. *J. Geophys. Res.*, 2010, **115**, D16302.
8. Sarangi, T. *et al.*, First simultaneous measurements of ozone, CO, and NO_y at a high-altitude regional representative site in the central Himalayas. *J. Geophys. Res. Atmos.*, 2014, **119**, 1592–1611.
9. Frehlich, R. G., Estimation of velocity error for Doppler Lidar measurements. *J. Atmos. Oceanic Technol.*, 2001, **18**, 1628–1639.
10. Ojha, N. *et al.*, On the processes influencing the vertical distribution of ozone over the central Himalayas: Analysis of yearlong ozonesonde observations. *Atmos. Environ.*, 2014, **88**, 201–211.
11. Grund, C. J., Banta, R. M., George, J. L., Howell, J. N., Post, M. J., Richter, R. A. and Weickmann, A. M., High resolution Doppler lidar for boundary layer and cloud research. *J. Atmos. Oceanic Technol.*, 2001, **18**, 376–393.
12. Pearson, G. N., Davies, F. and Collier, C., An analysis of the performance of the UFAM pulsed Doppler lidar for observing the boundary layer. *J. Atmos. Oceanic Technol.*, 2009, **26**, 240–250.
13. Rye, B. J. and Hardesty, R. M., Discrete spectral peak estimation in incoherent backscatter heterodyne lidar. I. Spectral accumulation and the Cramer-Rao lower bound. *IEEE Trans. Geosci. Remote Sensing*, 1993, **31**, 16–27.
14. Rye, B. J. and Hardesty, R. M., Discrete spectral peak estimation in incoherent backscatter heterodyne Lidar. II. Correlogram accumulation. *IEEE Trans. Geosci. Remote Sensing*, 1993, **31**, 28–35.
15. Pearson, G. N., Roberts, P. J., Eacock, J. R. and Harris, M., Analysis of the performance of a coherent pulsed fiber lidar for aerosol backscatter applications. *Appl. Opt.*, 2002, **41**, 6442–6450.
16. Banakh, V. A. and Smalikho, I. N., Estimation of the turbulence energy dissipation rate from pulsed Doppler lidar data. *Atmos. Oceanic Opt.*, 1997, **10**, 957–965.
17. Frehlich, R. G., Effects of wind turbulence on coherent Doppler lidar performance. *J. Atmos. Oceanic Technol.*, 1997, **14**, 54–75.
18. Browning, K. and Wexler, R., The determination of kinematic properties of a wind field using Doppler radar. *J. Appl. Meteorol.*, 1968, **7**, 105–113.
19. Newsom, R. K., *Doppler Lidar (DL) Handbook*, DOE/SC-ARM-TR-101; 2012; www.arm.gov/publications/tech_reports/handbooks/dl_handbook.pdf.
20. Banta, R. M., Newsom, R. K., Lundquist, J. K., Pichugina, Y. L., Coulter, R. L. and Mahrt, L. D., Nocturnal low-level jet characteristics over Kansas during CASES-99. *Boundary-Layer Meteorol.*, 2002, **105**, 221–252.
21. Barlow, J. F. *et al.*, Boundary layer dynamics over London, UK, as observed using Doppler lidar during REPARTEE-II. *Atmos. Chem. Phys.*, 2011, **11**, 2111–2125; doi: 10.5194/acp-11-2111-2011.
22. Shukla, K. K., Phanikumar, D. V., Newsom, R. K., Niranjan Kumar, K., Ratnam, M. V., Naja, M. and Singh, N., Estimation of the mixing layer height over a high altitude site in Central Himalayan region by using Doppler lidar. *J. Atmos. Solar-Terrestrial Phys.*, 2014, **109**, 48–53.
23. Grund, C. J., Nocturnal and transitional boundary layers observed by the high resolution Doppler Lidar during the LIFT experiment. Preprints. 12th Symp. on Boundary Layers and Turbulence, Vancouver, BC, Canada, *Am. Meteor. Soc.*, 1997, pp. 13–14.
24. Pearson, G. N. and Collier, C. G., A pulsed coherent CO_2 lidar for boundary–layer meteorology. *Q. J. R. Meteorol. SOC*, 1999, **125**, 2703–2721.
25. Kameyama, S., Ando, T., Asaka, K., Hirano, Y. and Wadaka, S., Compact all-fiber pulsed coherent Doppler lidar system for wind sensing. *Appl. Opt.*, 2007, **46**, 1953–1962.
26. Newsom, R. K. and Banta, R. M., Shear-flow instability in the stable nocturnal boundary layer as observed by Doppler lidar during CASES-99. *J. Atmos. Sci.*, 2003, **60**, 16–32.
27. Werner, C., Doppler wind lidar. Lidar: Range-resolved optical remote sensing of the atmosphere. *Ser. Opt. Sci.*, 2005, **102**, 339–342.

ACKNOWLEDGEMENTS. This work has been carried out as a part of the GVAX campaign in Joint collaboration among Atmospheric Radiation Measurement, Department of Energy (US), Indian Institute of Science and Indian Space Research Organization, India. We acknowledge late Dr P. Pant for his contributions during GVAX project. We thank Director, ARIES for providing the necessary support.

doi: 10.18520/cs/v111/i1/101-108